IEEE Access
Multidisciplinary | Rapid Review | Open Access Journal

Received October 15, 2020, accepted October 23, 2020, date of publication October 28, 2020, date of current version November 11, 2020.

Digital Object Identifier 10.1109/ACCESS.2020.3034275

A Hybrid Framework for Underwater Image Enhancement

XINJIE LI[1], GUOJIA HOU[1,2,3], (Member, IEEE), LU TAN[3,4], AND WANQUAN LIU[3], (Senior Member, IEEE)

[1]College of Computer Science and Technology, Qingdao University, Qingdao 266071, China
[2]School of Automation, Qingdao University, Qingdao 266071, China
[3]School of EECMS, Curtin University, Perth, WA 6102, Australia
[4]Department of Mathematics, Hong Kong Baptist University, Hong Kong

Corresponding author: Guojia Hou (hgjouc@126.com)

This work was supported in part by the National Natural Science Foundation of China under Grant 61901240, in part by the Natural Science Foundation of Shandong Province, China, under Grant ZR2019BF042, in part by the China Scholarship Council under Grant 201908370002, and in part by the China Postdoctoral Science Foundation under Grant 2017M612204.

ABSTRACT Underwater captured images often suffer from poor visibility caused by two major degradations: scattering and absorption. In this paper, we propose a hybrid framework for underwater image enhancement, which unifies underwater white balance and variational contrast and saturation enhancement. In our framework, the improved underwater white balance (UWB) algorithm is integrated with histogram stretching, aiming to better compensate the attenuation difference along the propagation path and remove undesired color castings. In addition, a variational contrast and saturation enhancement (VCSE) model is developed based on the enhanced result obtained from UWB. The advantages of VCSE model lie in the improvements of contrast and saturation as well as the elimination of hazy appearance induced by scattering. Moreover, we design a fast Gaussian pyramid-based algorithm to speed up the solving of VCSE model. The improvements achieved by our method include the more effective in color correction, haze removal and detail clarification. Extensive qualitative and quantitative assessments demonstrate that the proposed approach obtains high quality outcomes, which outperforms several state-of-the-art methods. Application tests further verify the effectiveness and broad application prospects of our proposed method.

INDEX TERMS Hybrid framework, dehazing, underwater white balance, variational contrast and saturation enhancement.

I. INTRODUCTION

With the increasingly serious problems caused by land resources shortage, population expansion and environmental deterioration, more and more research has focused on the utilization of marine resources. However, poor-visibility events are frequent in subsea image acquisition induced by complicated underwater imaging condition, leading to numerous obstacles for the exploration of marine resources. It is hence essential to develop a framework which allows for efficient and robust underwater image processing techniques to tackle the challenges of underwater imaging [1].

For the degradation problem of underwater images, numerous schemes have been proposed to improve the visibility and clarity of images, with great convenience for underwater exploration. According to whether relying on the underwater image formation model, the existing works are generally divided into two categories: underwater image enhancement and restoration [2]–[7]. These existing strategies may achieve good performance validated by objective evaluations, but without a comprehensive consideration about the multiple degradation and valuable information loss, resulting in limited applicable situations. With regards to restoration algorithms, they require additional prior knowledge about the imaging conditions, and are highly dependent on the correct prior hypotheses. However, it is difficult to generalize most scenes in the complicated and changeable underwater environment by a prior hypothesis like in the atmosphere. Thus, it may result in low robustness and produce poor results. As for enhancement algorithms, the generation of red artifacts is a common problem. To address these problems, we propose a novel variational framework for color correction, as well

The associate editor coordinating the review of this manuscript and approving it for publication was Gangyi Jiang.

as contrast and saturation enhancement. First, an improved underwater white balance (UWB) algorithm is developed on the basis of optical properties. Using this technique, the color castings caused by natural attenuation or artificial illumination can be eliminated, and the contrast loss induced by scattering is also compensated. Then, we establish a variational contrast and saturation enhancement (VCSE) model, wherein the result obtained from UWB will be regarded as a guidance to provide some essential prior reference information. In summary, our contributions mainly involve:

(1) An improved underwater white balance approach is proposed to reduce the error color estimation, in which the histogram stretching algorithm is successfully integrated to uniform three color channels.
(2) A variational model contained with a data term and two regularized terms is constructed, which needs only a few iterations to obtain a haze-free outcome.
(3) To accelerate the iterative efficiency, a fast Gaussian pyramid-based algorithm is designed to solve the proposed variational model.
(4) The proposed approach can provide a better performance in genuine color and stronger robustness versus other methods under different challenge scenes.

The major structure of this paper is organized as follows: Section I briefly introduces the underwater background and related work in this field. In section II, detailed description of the proposed approach is presented. Section III discusses the experimental results with qualitative and quantitative evaluation and comparisons against several representative dehazing techniques. Finally, the conclusion about our work is given in section IV.

II. BACKGROUND AND RELATED WORK

A. UNDERWATER IMAGE FORMATION MODEL

According to the comprehensive studies of underwater image formation model by McGlamery [8] and Jaffe [9], the total irradiance incident upon the image plane in underwater medium have three components including direct component, forward scattering and back scattering. The direct component is the light reflected directly by the object without being scattered in the water. The direct component at position x is written as:

$$E_D(x) = J(x)e^{-\tau d(x)} \tag{1}$$

where $J(x)$ is the radiance of target scene. $d(x)$ is the distance from the target scene to camera at coordinate point x. τ denotes the attenuation coefficient, which is related to the wavelength and is considered as a constant in a certain scenario.

For another two major causes of degradation, forward scattering and backward scattering, the former occurs when micro-particles in the medium change the path of light transmission. The negative influence comes down to random deviation or fuzzy edge. Generally, the effect of this component is approximated by a convolution of direct components. In contrast, the latter is caused by the fact that the camera has received lights reflected back by floating particles in water. It is usually modeled as:

$$E_{BS}(x) = B(x)(1 - e^{-\tau d(x)}) \tag{2}$$

where B is the back-scattered light.

In most cases, back-scattering is the main source of contrast loss and color distortion in underwater images, and the influence of forward-scattering is often ignored. Then, the total irradiance received by the device is simplified as:

$$I(x) = J(x)t(x) + B(x)(1 - t(x)) \tag{3}$$

where I is the total irradiance. J is the irradiation of target scene. t is the transmission map, which is used to represent $e^{-\tau d}$ in preceding equations.

Formally, the underwater image formation model of (3) resembles the atmospheric degradation model proposed by Koschmieder [10]. However, it ignores the fact that the attenuation rate of the component of light-ray propagating through water gradually decrease with the wavelength value rise, and this model is consequently defective.

B. RELATED WORK

Underwater images without any preprocessing can hardly be applied for further applications, such as image detection [11]–[13] and segmentation [14], [15]. There have been many explorations on improving visibility, enhancing contrast and recovering genuine color for underwater degraded images. In this subsection, we will make a brief review on these works.

The underwater image restoration methods utilize the latent parameters deduced by prior knowledge to invert the degradation process of underwater image, so as to recover the real scene radiation. The simplified image formation model of (3) is widely used due to its simplicity and effectiveness. Hou *et al.* [16] attempted to combine underwater optical attributes with traditional image restoration methods. Based on the assumption that the blur of underwater image is caused by light scattering due to water and suspended particles, underwater image deconvolution was implemented by estimating the parameters of light scattering. Carlevaris-Bianco *et al.* [17] estimated the depth of the scene by using the significant difference of attenuation among the three channels of underwater images. According to the obtained depth map, the influence of scattering can be suppressed. Lu *et al.* [18] developed a new underwater image formation model and applied wavelength compensation to restore the image captured in turbid water. Peng *et al.* [19] adopted image blurriness and light absorption to estimate the background light, scene depth, and transmission maps and restored more precise color. Berman *et al.* [20] analyzed the multiple spectral characteristics of various water conditions, and simplified the underwater image restoration to a single image dehazing problem by estimating two additional parameters. Wang *et al.* [21] proposed a restoration method based on

an adaptive attenuation-curve prior. To avoid over saturation and suppress noise, they further employ saturation constraints to adjust the transmission map.

As a special type problem of underwater image, dehazing has attracted much attention. In 2001, Schechner *et al.* [22] firstly adopted the polarization for haze removal. Afterward, Shen *et al.* [23] modified the imaging model by take into account the amplified noise, and then restore the degraded image relying on the correlation between the haze-free image and the transmission map. Recently, a series of dehazing techniques based on dark channel prior (DCP) have been investigated. This prior knowledge is first proposed by He *et al.* [24] in natural terrestrial image dehazing by calculating the amount of spatially homogeneous haze using the local minimum in three channels. Based on He's strategy, Liu *et al.* [25] optimized the estimation of depth map and the dehazed image by developing a framework based on the total generalized variation (TGV). Shu *et al.* [26] proposed a hybrid variational framework to improve the visual quality of the recovered image, especially for the sky region. Based on the combination of DCP and total variation model (TV), three kinds of variation framework were proposed in [27] for image dehazing and denoising. DCP can be seen as a celebrated breakthrough in this field. Due to the similarity of optical image formation model in underwater and atmosphere, this prior also provided a new solution for the underwater dehazing. Chiang and Chen [28] restored underwater images by integrating a dehazing algorithm into a wavelength compensation. Drews, Jr., *et al.* [29] proposed an underwater dark channel prior (UDCP) on the basis of hypothesis that the visual information under the water predominantly originate from the blue and green color channels. Galdran *et al.* [30] noticed the red component reciprocal increases with the distance to the camera, and introduced a red channel prior (RCP) which can be seen as a variant of dark channel prior to recover colors associated with short wavelengths. Peng *et al.* [31] introduced an adaptive color correction into an image formation model, and proposed a generalized dark channel prior (GDCP). In [32], a novel variational framework incorporating the RCP and quad-tree subdivision to estimate transmission map and back-scattered light was proposed.

Distinguishing from restoration method, underwater image enhancement method relies on the information extracted from the image to adjust the pixel value. These approaches are diverse and versatile, most of them aim to increase the visibility and sharpness to improve the image quality. In the earlier research stage, traditional image enhancement methods usually performed well in ordinary atmospheric images. But for underwater images with more complicated features, it was rather difficult for these traditional enhancement methods to acquire satisfactory results. For example, when classical histogram equalization and its variants [33], [34] were applied for underwater images, severe artifacts and amplified noise on the propagation path of light appeared. As for the images with insufficient light intensity, the implementation of Gray-world hypothesis [35] and some traditional white balance algorithms [36] may lead to serious color distortion. In addition, the Gray-edge assumption [37] will lose its rationality due to the low contrast and the lack of visual edge. Despite of some domain-transform methods [38]–[40] could effectively suppress noises for underwater images, they failed to solve the problems of contrast loss and color deviation. In a word, the traditional image enhancement methods can hardly deal with the multiple degradation of underwater image without analyzing the internal factor.

As underwater image processing techniques have attracted more attention in recent years, many researches have been developed to tackle the shortcomings of traditional enhancement methods. Iqbal *et al.* [41] adopted the histogram stretching both on RGB and HSI color space to improve color deviation and contrast with promising results. In [42], Ancuti *et al.* utilized a fusion principle to improve the quality of underwater image by four weight maps: brightness, contrast, chroma and saliency. The color-corrected version and the contrast-enhanced version of the original image were fused at multi-scale to obtain enhanced results. Fu *et al.* [43] extracted the CIELab spatial luminance component from the color-corrected underwater image by a Retinex-based variational framework. Ji *et al.* [44] enhanced the degraded images based on image structure decomposition, and also solved the problem of uneven illumination within underwater image on the premise of preserving some details and structure. Ghani and Isa [45], [46] exploited a series of color correction strategies, the color deviation was reduced via Rayleigh distribution, while the contrast and saturation was upgraded by stretching corresponding components in HSV space. In [47], a two-step approach was proposed for underwater image enhancement including color correction and contrast enhancement. In [48], Li *et al.* developed a single underwater image enhancement method based on minimum information loss and histogram distribution prior. The proposed technology is combined with a dehazing algorithm and a contrast enhancement algorithm. Afterward, Li *et al.* [49] introduced a weakly supervised color transfer method to cope with Perceptual distortion. Very recently, Ancuti *et al.* [50] proposed a two-step fusion strategy combing white balance algorithm and image fusion algorithm, which can effectively correct the color deviation for underwater images.

In this work, we develop a hybrid variational framework to enhance the underwater degraded images. The proposed strategy can generate two versions of enhanced outcome. One version with vivid color and natural appearance is used as a guided image. The other version is the obtained haze-free output with contrast and saturation enhancement. Additionally, compared with the existing single image enhancement algorithms and dehazing algorithms, the proposed approach does not tend to introduce red artifacts, and is more robust to various challenge underwater scene. Actually, our method can achieve visually pleasing outcome even for the underwater image with serious light attenuation. Compared with existing methods in dependence of multiple images or specialized

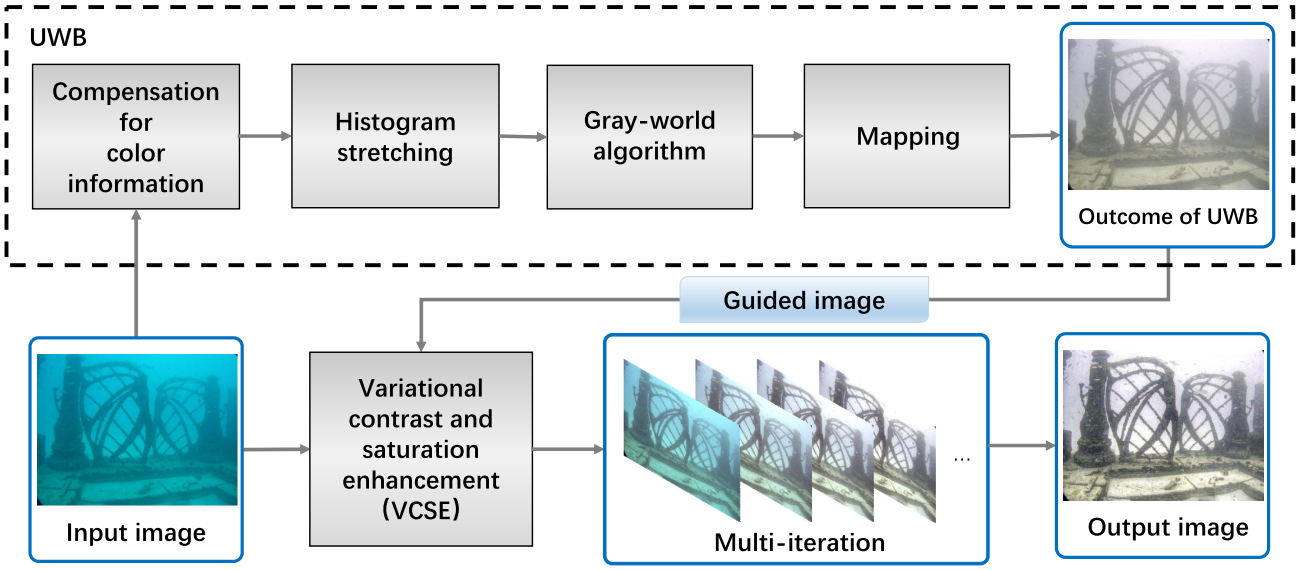

FIGURE 1. Flowchart of the proposed method.

hardware, the proposed method is designed for single image enhancement without requiring multiple images or additional knowledge about underwater environment.

III. PROPOSED METHOD

The proposed approach consists of two parts, underwater white balance and variational contrast and saturation enhancement. One flowchart illustrates the detailed procedure in Fig. 1.

A. UNDERWATER WHITE BALANCE

It is well known that the traditional white balancing methods mostly estimate the color of light source by a specific assumption, then achieve the color constancy by dividing each color channel into corresponding normalized light source intensity. Despite of their good performance for out-doors images, this assumption often fails if underwater image suffers from some color deviation. In addition, the classical gray world algorithm assumed that the mean reflectance of the scene is achromatic, and one estimated the color distribution of the light source by averaging each channel separately. This strategy performs well in removing color deviation. However, when it is directly applied to the underwater images, a certain degree of artifacts will be introduced due to over compensation, especially for serious color deviation area. In order to avoid this problem, it is necessary to compensate the color loss before applying this strategy.

In [50], Ancuti *et al.* presented four principles to compensate the loss of red channel. Here, we extend them with another two observations: a) In some turbid waters or areas with high concentration of plankton, the blue components often suffer from severe attenuation. Thereby, compensating the attenuation of blue and red components simultaneously can be more applicable for various underwater environments; b) For the problem of insufficient or excessive compensation, combing histogram stretching can assure the distributions of the three color channels by the uniform information in the whole region, and reduce the error compensation.

Based on these observations, an integrated strategy combining additive compensation and histogram stretching is proposed, which can restore the intensities of decaying channels. Its mathematical expression is as follows:

$$I_{w1,c}(x) = I_c(x) + \eta(\bar{I}_g - \bar{I}_c)(1 - I_c(x))I_g(x) \tag{4}$$

$$I_{w2,c} = (I_{w1,c} - a)(\frac{c-d}{b-a}) + d \tag{5}$$

where c denotes the color channels, $c \in \{R, G, B\}$. I is the initial image. $\bar{I}$ represents the average value of three color channels of I. η is a regulation parameter, usually assigned to 1. a is limited lower pixel value and b is the upper one. c and d represent the maximum and minimum values of intensity respectively. Given an input image I_{w1}, the values of a, b, c, d can be fixed.

To simplify the implementation process by designing an integrated operation, the compensation of multiple channels is coupled in a unified formula (4). After compensating for the attenuation, the following Gray-world assumptions (6-9) can be used to correct the color distortion:

$$\overline{Gray} = \frac{\sum_c \sum_{x\in\Omega} I_{w2,c}(x)}{3} \tag{6}$$

$$p_c = \frac{\overline{Gray}}{\sum_{x\in\Omega} I_{w2,c}(x)} \tag{7}$$

$$I_{w3,c} = p_c I_{w2,c} \tag{8}$$

$$I_{W,c} = \begin{cases} 1 & I_{w3,c} > 1 \\ I_{w3,c} & 0 \le I_{w3,c} \le 1 \\ 0 & I_{w3,c} < 0 \end{cases} \tag{9}$$

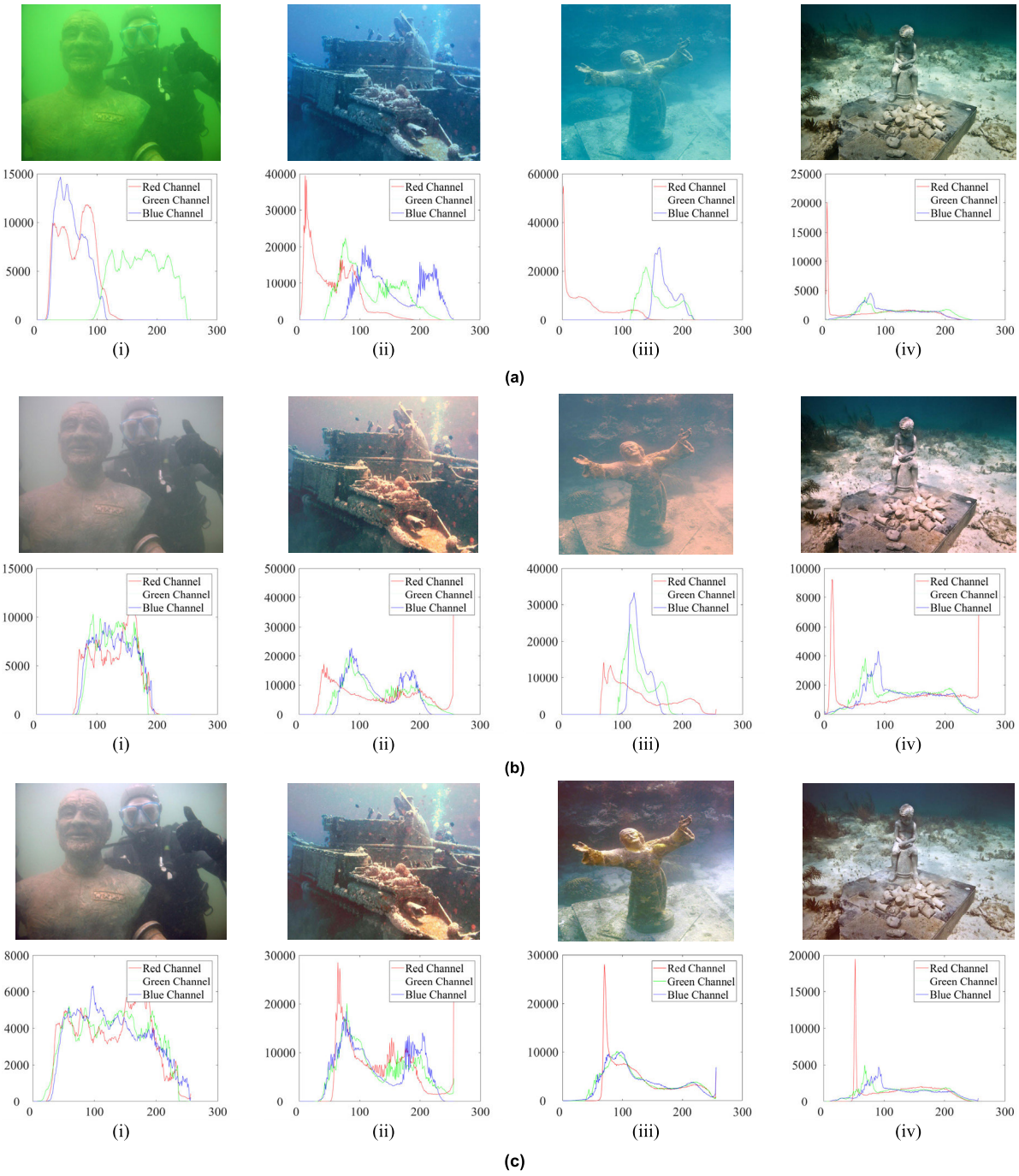

FIGURE 2. Comparisons of histogram distribution of R, G, B channels. (a) Raw images, (b) the results of Ancuti et al. [50], (c) the results of proposed UWB strategy.

where I_{w3} is the result of Gray-world algorithm. I_W is the output of UWB strategy, Ω refers to the whole image area.

In order to illustrate the improvement of the proposed UWB, the results of Ancuti *et al.* and ours are presented, as well as the related histogram distribution in Fig. 2. Visually, the method of Ancuti *et al.* is prone to over enhance the red channel, resulting in an unnatural red tone of the outcomes. Here we can easily observe from Fig. 2(b) that the red component of Ancuti *et al.* has the more concentrated distributions in high gray level than the blue and green components. Moreover, their approach seems to aggravate the back scattering. Compared with the strategy of Ancuti *et al.*, our method can effectively eliminate the color cast and achieve more visual pleasing results. Also, the more uniform histogram distribution of our enhanced results represents a better balance between the three components, with no one

TABLE 1. Color cast detection on raw images, comparison results of Ancuti *et al.*'s method and our method. The last column is of 50 randomly selected images extracted from the underwater benchmark dataset [52].

	(i)	(ii)	(iii)	(iv)	AVG
Raw	246.17	65.84	53.64	13.46	87.51
Ancuti et al.	3.79	3.25	2.21	2.69	2.74
Ours	1.20	0.48	0.39	0.64	0.85

dominating. Since the loss of color intensity has been compensated adaptively before stretching, our results refrain from the quantized artifacts resulted from direct domain stretching of degraded image. In addition, our UWB method further shrinks the difference among the three color channels and reduces the error compensation. This guarantees our proposed strategy become more robust when applied to various underwater environments, even in the extreme deteriorated scenarios.

To further verify the color accuracy of enhanced result, a color deviated detection [51] is employed to objectively assess it. Table 1 first presents the comparative results associated to the Fig. 2. Besides, we conduct a broader test using 50 raw images randomly selected from the underwater benchmark dataset [52]. Their corresponding average scores are given in the last column of Table 1, where smaller values indicate the color performance is better. It can be easily seen that the scores of our results are significantly lower than that of Ancuti *et al.*, and are far less than the raw degraded images. Thus, the effectiveness and superiority of our improved strategy is well demonstrated.

B. VARIATIONAL CONTRAST AND SATURATION ENHANCEMENT

Although our UWB method has a good performance on color correction, which is insufficient to obtain the desired results. In order to restore more visibility, inspired by automatic contrast enhancement (ACE) [53], we further develop a variational model with a data term and two regularized terms for contrast and saturation enhancement. The data term attempts to prevent the output image departing from restored color by penalizing difference between u and white balancing result I_W. The two regularized terms are exploited to enhance image in different aspects. One is used to measure the contrast by calculating the weighted differences between each pixel with global background in one single channel, and the other one intends to improve the saturation by enlarging the difference among the R, G, B components. For each channel, the formula is given as:

$$\begin{aligned} E(u_c) = & \frac{1}{2}\sum_{x}\left(u_c(x) - I_{W,c}(x)\right)^2 \\ & -\frac{\alpha}{2}\sum_{x,y} w(x,y)S\left(u_c(x) - u_c(y)\right) \\ & -\frac{\beta}{2}\sum_{x,y}\left((u_c(x) - u_{c+1}(x))^2 + (u_c(x) - u_{c+2}(x))^2\right) \end{aligned} \tag{10}$$

where the $c \in \mathbb{R}_3$, means the space of integers modulo 3 (i.e. $I_1 = I_R, I_2 = I_G, I_3 = I_B$). u is the enhancement result, I_W is the guide image obtained from the proposed UWB, α are two positive parameters, w denotes a distance-dependent weight. S is a turning function.

Here, w is used to weight the amount of local contribution. This weight function is introduced to balance the filtering effect of pixels near the border and avoid the halo appearance around the edge caused by back-scattering. For any two points x, y that is non-coincident on a single channel, w is given as follows:

$$w(x,y) = \frac{A(x)}{\|x - y\|}, \quad x \neq y \tag{11}$$

$$with \;\; A(x) = \left(\sum_{y\in\Omega}\frac{1}{||x - y||}\right)^{-1} \tag{12}$$

S is a transformation from the primitive function of sigmoid function, it can be formally regarded as a smoothed version of absolute value function, as shown in Fig. 3. Its expression is given as:

$$S = x + \frac{2\ln(e^{-\lambda x} + 1)}{\lambda} \tag{13}$$

$$s(x) = S'(x) = \frac{2}{1 + e^{-\lambda x}} - 1 \tag{14}$$

where λ is a parameter used to adjust the slope. s represents the derivative of function S.

Here, S is used to tune the relative difference of the intensity between $u_c(x)$ and $u_c(y)$. As shown in the Fig. 4, the chromatic adaptation function S is derivable everywhere in the definition domain. After the absolute value reaches 1, the first-order derivative s will remain stable. At this moment, the S function can be regarded as a part of the signal function. In another case, while the absolute value of slope is less than 1, S is designed to limit the over enhancement by decreasing the slope. The function S can amplify the small difference and saturate the large difference, which has the ability of expanding or scaling the dynamic range based on the local image information. Besides, the derivative adopted smooth sigmoid function s assures that the contribution of relative differences is conform to the principle of human visual perception. By altering the slope, we are able to control the effect of contrast enhancement. The larger value of λ is, the more significant improvement can be achieved in the low-contrast region. Until the value of λ is infinitely large, S will completely evolve into a signal function. It can be observed that our VCSE algorithm is integrated with the

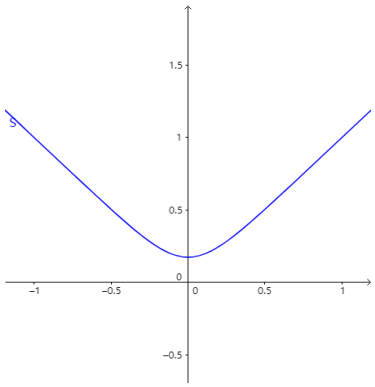

FIGURE 3. The *S* function.

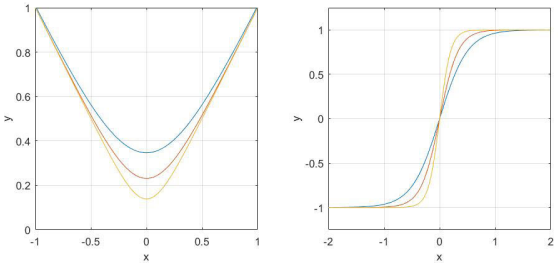

FIGURE 4. The *S* function with different values of ratio λ (left) and its corresponding *s* function (right).

data term and regularized terms to construct a competitive relationship between them. The minimization of the energy (10) means the suppression for the first term and the increasing of the second and third terms. After a limited number of iterations, an output image with enhanced contrast and saturation and ameliorated tones can be gained.

For numerical implementation, we adapt gradient descent strategy to minimize (10). In the first step, we need to compute its Euler-Lagrange derivative. Given u is the enhanced image, then we can obtain:

$$\begin{aligned}\delta E(u_c) = &(u_c(x) - I_{W,c}(x)) - \alpha R_c(u_c)(x) \\ &-\beta\left(2u_c - u_{c+1} - u_{c+2}\right) = 0, \qquad (15)\end{aligned}$$

$$R_c\left(u_c\right)(x) = \sum_{x,y\in\Omega} w(x,y)s\left(u_c(x) - u_c(y)\right) \qquad (16)$$

Now we use gradient descent strategy to solve it. Starting from initial image, we need to solve:

$$\frac{\partial u}{\partial t} = -\delta E(u) \qquad (17)$$

where t denotes the timeline. In order to discretize (17) by using an explicit scheme, it can be rewritten as:

$$\begin{aligned}\frac{u_c^{k+1}(x) - u_c^k(x)}{\Delta t} = &(I_{W,c}(x) - u_c^k(x)) + \alpha R_c^k(u_c)(x) \\ &+\beta\left(2u_c^k(x) - u_{c+1}^k(x) - u_{c+2}^k(x)\right) \qquad (18)\end{aligned}$$

where k denotes the number of iterations. $I_0 = I$ represents the initial image. After a simple transposition of (18), we have the rules of iteration are presented as:

$$\begin{aligned}u_c^{k+1} = &u_c^k\left(1 - \Delta t(1-2\beta)\right) \\ &+\Delta t\left(I_{W,c} + \alpha R_c^k\left(u_c\right) - \beta u_{c+1}^k - \beta u_{c+2}^k\right) \qquad (19)\end{aligned}$$

where $0 < \Delta t \leq 1/(1-2\beta)$.

The proposed algorithm is terminated when the energy in (10) is reduced to steady state. For the calculation of operator R, it is tedious and unrealistic to calculate it directly. Here, we utilize a multi-resolution strategy to solve it. Firstly, the input image is gradually subsampled to construct a Gaussian pyramid. Defining a sliding window, the value of centered pixel is obtained by normally calculating R within the window range. Using this way, the global computational information is approximated by calculating the minimum thumbnail at the top of the pyramid. Then, from above to below, the incomplete detailed information contained in neighboring areas is updated layer by layer. Details are presented in Algo. 1. By applying this strategy, we only need to calculate the difference between each pixel and its adjacent pixels, rather than with the whole image, thus greatly reducing the cost of computing (16). Experimental results show that for a 720 × 1280 color image, the processing time is decreased from 212s to 45s after using the accelerated algorithm, which proves the effectiveness of our speed-up method.

IV. RESULTS DISCUSSION AND EVALUATION

In this section, in order to assess the effectiveness of the proposed method, we analyze the experimental results on some natural underwater images, and discuss the performance between the proposed method and some existing research. The baseline configuration of our approach is set as $\Delta t = 0.5$, $\alpha = 0.2$, $\beta = 0.06$, $\lambda = 6$. Note that all the experiments are implemented in MATLAB 2016b on an Intel 3.33GHz PC with 8GB RAM.

A. EXPERIMENT RESULTS

Due to the application of gradient descent strategy, the processing procedure of the proposed approach seems to be multistage and gradually transitive, which allows us to control the degree of scene restoration. In fact, it is also the advantage of variational framework and gradient descent methods to better illustrate the processing flow. The intermediate results in evolution and the convergence curve are shown in Fig. 5. Moreover, we also calculate the indictor namely fog density (FD) [54] to demonstrate the ability of our proposed approach for dehazing. Their corresponding FD values are rendered in the upper right of the restored image. In Fig. 5(b)-(h), we can see the FD score shrinks very quickly in the first few iterations, and then slowly drops to a relatively low value. From Fig. 5(i), it also can be seen that the energy of proposed method has a faster decline rate in the early stage, and will be stable after a limited number of iterations. When the energy drops extremely small, the computation stops and the dehazing image at this time is recorded as the final output. The sufficient experimental results demonstrate

Algorithm 1 Fast computing for R

Input parameter: input color image u, ratio λ.
Output parameter: R.

Function Main(u, λ)
  for $c \in \{R, G, B\}$**do**
  $R \leftarrow$ Recursion(u_c, λ);
  end for
  return R
end function

Function Recursion(P_{mono}, λ)
  if size(P_{mono}) $\leq$ 2**do**
    return zeros(**size**(P_{mono}));
  end if
  $Rh \leftarrow$ **resize** (P_{mono}, **size** (P_{mono})/2);
  $Ra \leftarrow$ Recursion (Rh, λ);
  $Rh \leftarrow$**resize**(Rh, **size**(P_{mono}));
  $Ra \leftarrow$**resize**(Ra, **size**(P_{mono}));
  $Ru \leftarrow Ra+$ Computing(P_{mono}, λ)
    - Computing(Rh, λ);
  return Ru
end function

Function Computing (P_{mono}, λ)
  Define a sliding window with radius λ;
  Normally compute the R within the window range to obtain the value of centered pixel;
  return the computational result of whole image P_{mono};
end function

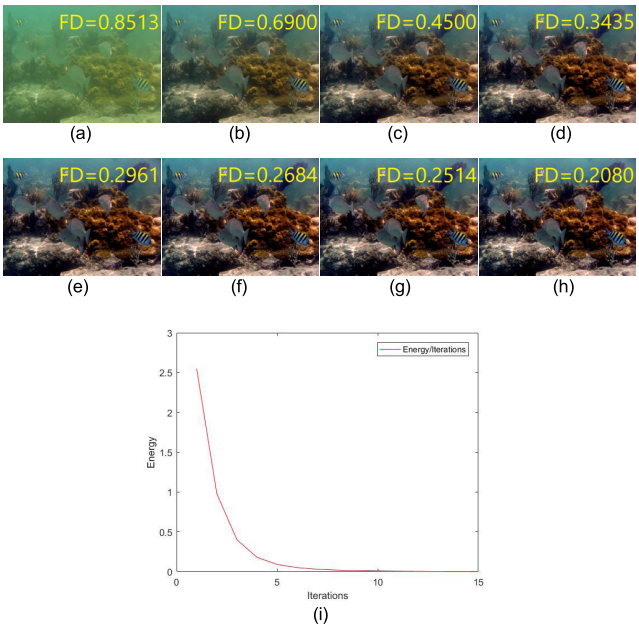

FIGURE 5. Iteration results. (a) Raw image, (b-g) corresponds to the intermediate results with $k = 1 - 6$, (h) the final output, (i) the convergence curve of function energy.

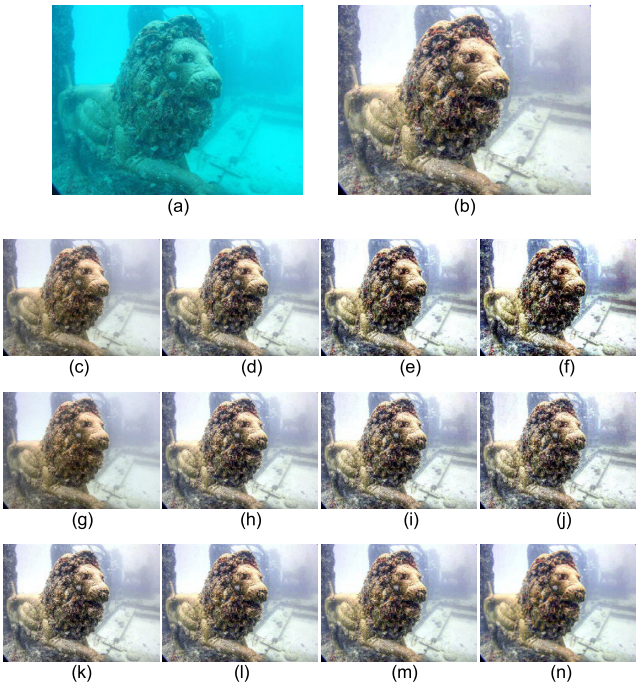

FIGURE 6. Outputs with different parameter settings. (a) Raw image, (b) the output with configuration $\alpha = 0.2$, $\beta = 0.06$, $\lambda = 6$, (c-f) the corresponding output with $\alpha = 0.1, 0.2, 0.3, 0.4$ and $\lambda = 6$, $\beta = 0.06$, (g-j) the corresponding output with $\lambda = 2, 6, 8, 10$ and $\alpha = 0.2$, $\beta = 0.06$, (k-n) the corresponding output with $\beta = 0.02, 0.06, 0.10, 0.14$ and $\lambda = 6$, $\alpha = 0.2$.

that our variational framework method can obtain a satisfying outcome.

Next, the effect of varying parameter settings is discussed. We choose a degraded underwater image with blueish scene for sample, as shown in Fig. 6(a). Fig. 6(b) presents the corresponding final output of our proposed method using the baseline configuration. The α and λ are both related to enhancing the contrast, but the modification on them will yield different outcomes. The α controls the proportion of the contrast terms in the energy function, which has a prominent effect on global contrast enhancement. To illustrate this, the proposed method is executed by fixing $\lambda = 6$, $\beta = 0.06$ and setting $\alpha = 0.1,\ 0.2,\ 0.3,\ 0.4$ respectively. The experimental results are displayed in Fig. 6(c-f). It can be found that when α is set to a small value 0.1, the color of the enhanced image is obviously changed, but the haze is removed. Subsequently, as the α increasing from 0.1 to 0.4, the global contrast is gradually improved, and the hazy-appearance is also mitigated. However, the enhancement of global contrast also amplifies the brightness difference in varying areas. This effect can no longer be ignored in the result when $\alpha = 0.4$, since some areas become too dark or too bright to see the details. Therefore, to avoid the loss of visual information, the value of α should be reasonably limited. In general, we set the value range as (0, 0.3].

On the contrary, the λ is a parameter exploited to control the amplification of difference between pixels and channels,

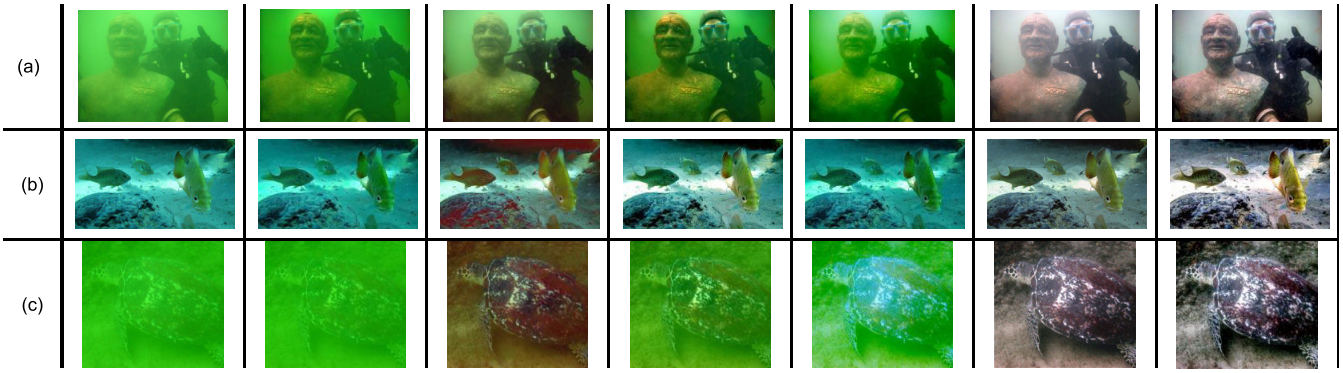

FIGURE 7. Comparison of the enhanced results generated from underwater images with greenish scene. From left to right are raw images and outputs obtained using: UDCP [29], RCP [30], Wavelet-based [55], IBLA [19], Fusion-based [50] and proposed method, respectively.

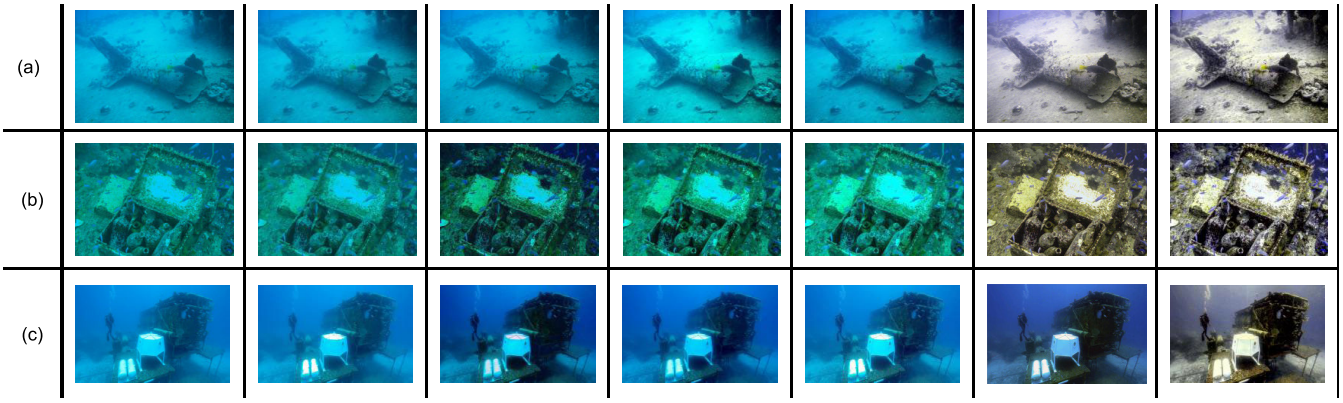

FIGURE 8. Comparison of the enhanced results generated from underwater images with blueish scene. From left to right are raw images and outputs obtained using: UDCP [29], RCP [30], Wavelet-based [55], IBLA [19], Fusion-based [50] and proposed method, respectively.

hence it has a close connection with the local contrast. We can appreciate how the different λ settings affect the results by focusing on the Fig. 6(g-j), where the λ is set to 2, 6, 8, 10 separately and fix $\alpha = 0.2$, $\beta = 0.06$. We see from there more details of sculpture are unveiled as the λ increased. But also, a little noise amplification and distortion can be noted when λ is taken as a relative high value. Hence, similar to α, λ is generally set as $0 < \lambda \leq 8$.

β is the coefficient of saturation term. By adjusting it, users are allowed to alter the saturation enhancement of enhanced image. In Fig. 6(k-n), we conduct some tests with the configurations of $\alpha = 0.2$, $\lambda = 6$, and varying β in the set $\{0.02, 0.06, 0.10, 0.14\}$. The improvement on saturation can be clearly seen in Fig. 6(k-n), in which the statue becomes more yellow as the β increases. In fact, for most cases, the saturation loss caused by back-scattering is very small. To avoid over compensating the color, the value of β should be relatively small, usually set as 0.06.

Regarding the above discussion, it can be concluded that our declared configuration in the beginning can better strike the balance of visibility, noise and colorfulness. Therefore, these parameter settings are also used in the following experiments, unless otherwise specified.

B. QUALITATIVE ASSESSMENT

In this section, the proposed method is compared with several state-of-the-art enhancement and restoration techniques (*i.e.* UDCP [29], RCP [30], Wavelet-based [55], IBLA [19], and Fusion-based [50]. Since the absence of ground-truth in underwater environment, the assessment for underwater image quality usually employs two strategies: subjective evaluation and no-reference objective evaluation. For the objective evaluation, we measure it by using several recent non-reference metrics (*i.e.* UCIQE [56], UIQM [57], PCQI [58] and MEON [59]).

As shown in the Fig. 7-11, we choose several underwater degraded images captured in different challenge scenes (greenish, blueish, turbid, low-light and with artificial lighting) for comparison. Fig. 7 gives a group of greenish underwater images, which seems to be the most common cases in coastal waters. It is clear that RCP method, Fusion-based method, and the proposed method all significantly improve the visibility. But among them, only the proposed method and Fusion-based method can restore more vivid colors. In contrast, RCP method has the problem of introducing excessive red color appeared in the restored result, as shown in the third column of Fig. 7(b). Similarly, UDCP algorithm aggravates the green tones that is originally appeared in the image.

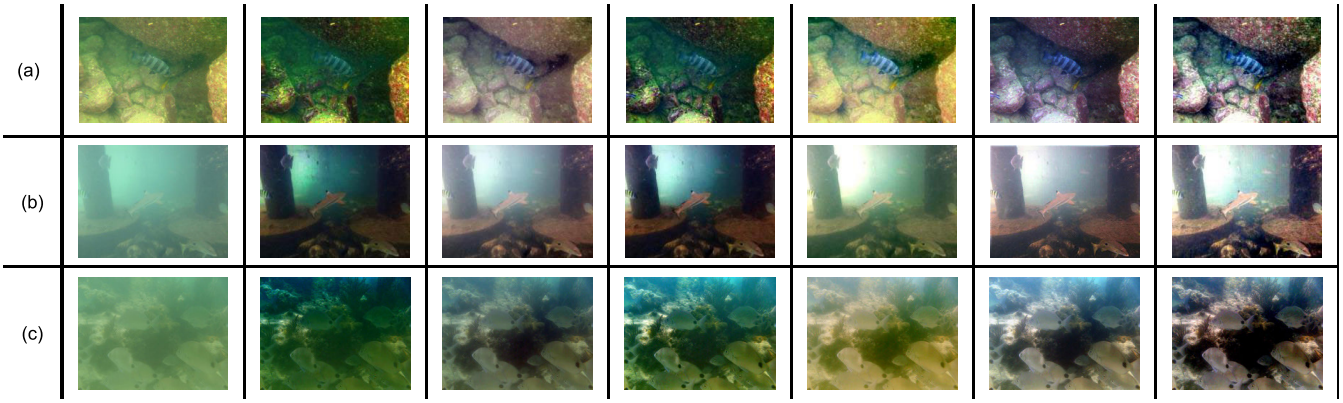

FIGURE 9. Comparison of the enhanced results generated from underwater images with turbid scene. From left to right are raw images and outputs obtained using: UDCP [29], RCP [30], Wavelet-based [55], IBLA [19], Fusion-based [50] and proposed method, respectively.

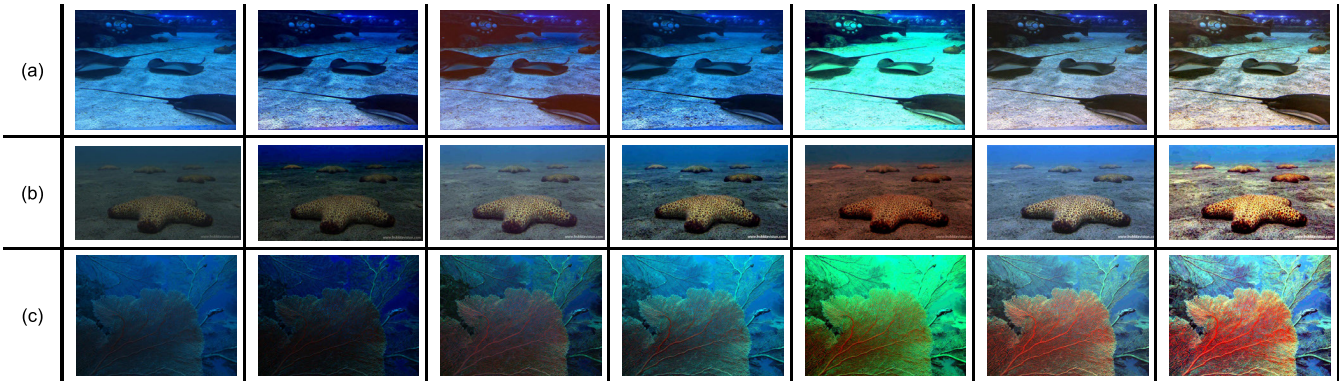

FIGURE 10. Comparison of the enhanced results generated from underwater images with low-light scene. From left to right are raw images and outputs obtained using: UDCP [29], RCP [30], Wavelet-based [55], IBLA [19], Fusion-based [50] and proposed method, respectively.

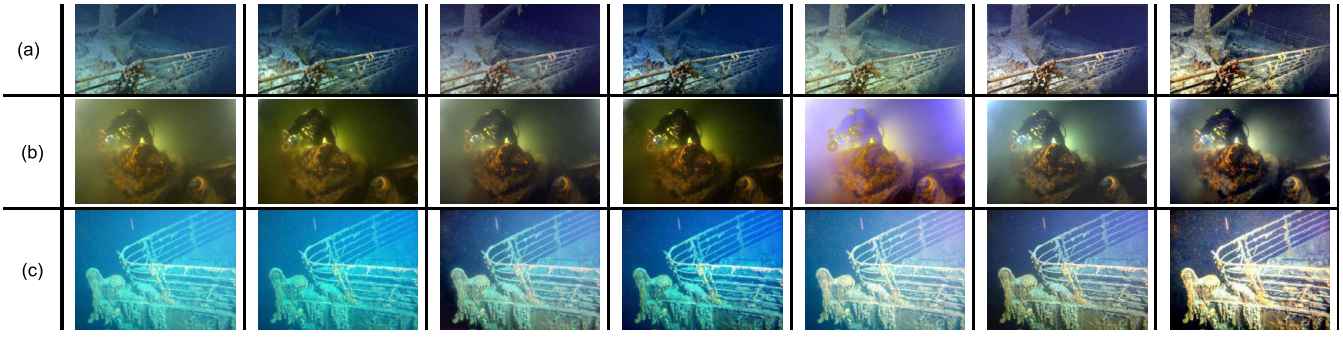

FIGURE 11. Comparison of the enhanced results generated from underwater images with artificial lighting scene. From left to right are raw images and outputs obtained using: UDCP [29], RCP [30], Wavelet-based [55], IBLA [19], Fusion-based [50] and proposed method, respectively.

Both Wavelet-based and IBLA methods fail to reveal scene features, and neither of them can correct the overall tones of the image.

The blueish image is a challenging and tough situation for most underwater dehazing methods. In this scenario, the green channel is unable to maintain its intensity, which cannot provide sufficient useful information for image enhancement or restoration. From Fig. 8, it can be observed that UDCP, RCP, Wavelet-based, and IBLA methods have little effect on solving this problem. Fusion-based approach plays a role in color correction, but it seems to have less robustness, as shown in penultimate column of Fig. 8. Fortunately, the obtained results of the proposed method succeed in tackling this issue, which unveil more details and achieve a satisfactory color performance.

In turbid waters scene, the negative effects caused by scattering become more prominent. In this case, it can provide a good chance for these compared methods to evaluate their performance on dehazing. The corresponding recovered results generated from three representative underwater

images captured under turbid scenes are presented in Fig. 9. Actually, the classic DCP algorithm plays a role in haze removal, variants of this algorithm like UDCP and IBLA can also remove the foggy appearance to a reasonable extent. But both these two approaches will degrade the overall brightness in the image, resulting in the unpleasing visual results. Similar to RCP algorithm, the results produced by Fusion-based algorithm prone to whitening the target scenario. Besides, the lack of sharpness is an obstacle for them to uncover some details. Unlike these methods, the recovered results generated by our algorithm is superior in dehazing against these methods, especially for keeping the color fidelity.

For the low-light scene, besides the color cast and scattering, restoring the illumination is another problem need to be solved. As shown in Fig. 10, the UDCP method reduces the brightness of images, while the IBLA obviously over enhance the red and green channel and consequently introduce some additional color deviation. The RCP, Wavelet-based and Fusion-based methods can slightly improve the visibility, but their results are still unsatisfactory. On the contrary, our proposed approach shows more effectiveness in color correction and illumination recovery, as well as unveil more details hidden in the dark area.

Underwater image with artificial lighting is a special kind but not rare case. In some water areas, the light from natural source is blocked or attenuated, so the assistance of artificial light is necessary. Due to the different light attenuation rates in the artificial lighting area, the ability to isolate its interference and correctly restore or enhance the image is the key criteria to assess the robustness of the underwater dehazing techniques. Since Wavelet-based method and UDCP method initially do not take this situation into account, their experimental results are not as satisfactory as expected, which are shown in Fig. 11. RCP algorithm reasonably avoided the influence of this area, but the retorted effect of the whole image is not obvious. Unlike RCP, IBLA algorithm fails to avoid the problem of over enhance due to the non-uniform illumination. Fortunately, both the Fusion-based algorithm and our proposed method can better moderately brighten the image and enhance the contrast in the dark regions. Comparing with the Fusion-based method, it can be found that the proposed method can reveal more accurate details and sharp the edge contour. In order to illustrate this superiority in detail, we give several other examples with more texture structure in Fig. 12. The difference between the Fusion-based method and our method can be determined visibly. In each original and restored image presented in Fig. 12, we further provide magnified details in the left bottom corner. Obviously, the proposed method achieves a sharper edge performance and reveals more details than Fusion-based method.

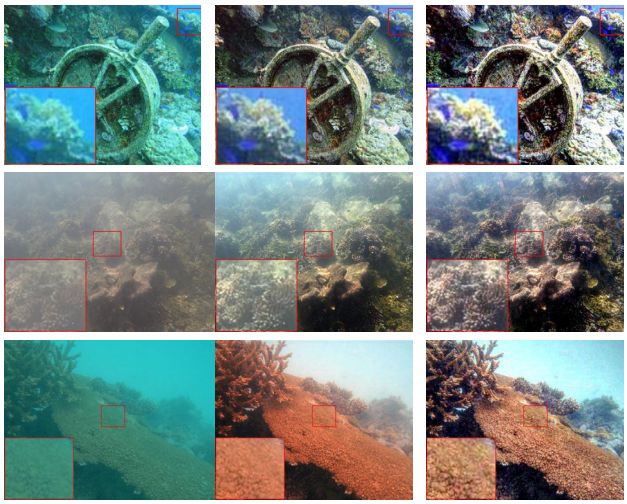

FIGURE 12. Comparison of the enhanced results generated from underwater images with textured details. From left to right are: raw images, outputs obtained using Fusion-based [50] and outputs of the proposed method. The left bottom of each image shows the result of magnified details in the box.

C. QUANTITATIVE ASSESSMENT

For the quantitative assessment, we employ several objective metrics including UIQM, UCIQE, PCQI, and MEON which are widely used to evaluate the performance. PCQI metric is used to evaluate the perceptual distortion of image by decomposing image into average intensity, signal intensity and signal structure components via adaptive representation of local patches. MEON metric relies on a distortion type identification sub-network and a quality prediction sub-network to blindly assess the image quality. Despite that PCQI and MEON are general-purpose metric for image contrast evaluation, UIQM and UCIQE metrics are specially designed for underwater image evaluation. UIQM quantifies image quality via a linear combination of colorfulness (UICM), sharpness (UISM) and contrast (UIQM), while UCIQE metric focuses on the quantification of nonuniform color cast, blurring, and low-contrast which characterize underwater images.

The quantitative assessment results generated from Figs. 7-11 by the five compared methods and the proposed approach are shown in Table 2. For all metrics, the larger values present the better results. With regards to the greenish image and artificial lighting image, it can be observed that our method acquires almost the best score in terms of all metrics due to its outstanding performance in enhancing contrast and restoring vivid color. For blueish images, since UDCP, RCP, and Wavelet-based methods are all derived from DCP algorithm, their PCQI scores are generally approach to 1, which means they have little effect in contrast. Despite of the better performance of Fusion-based in terms of UCIQE and UIQM, it is valueless when considering its low robustness and color accuracy. In the turbid water and low-light scene, the produced outcomes by UDCP and Wavelet-based methods contain many dark areas. Besides, their occasional high values of UCIQE and UIQM are abnormal, which are inconsistent with the subjective perceptual evaluation. Even so, the proposed method still obtains high quality against other compared methods in terms of PCQI and MEON metrics.

TABLE 2. Quantitative assessments of the restored images presented in Figs. 7-11 using UCIQE [56], UIQM [57], PCQI [58], MEON [59] metrics. (The bold values express the best metric values).

Assessments for underwater images with greenish scene (Fig. 7)																								
	UDCP				RCP				Wavelet-based				IBLA				Fusion-based				Proposed method			
	UCIQE	UIQM	PCQI	MEON	UCIQE	UIQM	PCQI	MEON	UCIQE	UIQM	PCQI	MEON	UCIQE	UIQM	PCQI	MEON	UCIQE	UIQM	PCQI	MEON	UCIQE	UIQM	PCQI	MEON
(a)	0.46	0.73	0.62	12.1	0.55	0.85	0.68	15.1	0.55	0.92	0.63	13.5	0.56	0.87	0.65	13.9	0.57	0.95	0.74	13.2	**0.58**	**1.37**	**0.96**	**15.2**
(b)	0.32	0.64	0.94	17.4	0.50	1.21	1.03	19.1	0.40	0.99	1.12	18.8	0.49	1.11	1.17	19.3	0.59	1.06	0.98	19.1	**0.60**	**1.54**	**1.33**	**24.1**
(c)	0.58	1.03	0.92	33.3	**0.65**	1.06	0.89	22.3	0.59	1.09	0.95	18.7	0.63	1.19	1.07	25.8	0.54	1.38	1.27	33.4	0.62	**1.42**	**1.17**	**40.0**
Average	0.45	0.80	0.83	20.9	0.57	1.04	0.87	18.8	0.51	1.00	0.90	17.0	0.56	1.06	0.96	19.7	0.57	1.13	1.00	21.9	**0.60**	**1.44**	**1.16**	**26.5**
Assessments for underwater images with blueish scene (Fig. 8)																								
	UDCP				RCP				Wavelet-based				IBLA				Fusion-based				Proposed method			
	UCIQE	UIQM	PCQI	MEON	UCIQE	UIQM	PCQI	MEON	UCIQE	UIQM	PCQI	MEON	UCIQE	UIQM	PCQI	MEON	UCIQE	UIQM	PCQI	MEON	UCIQE	UIQM	PCQI	MEON
(a)	0.47	0.95	0.98	13.5	0.47	1.43	1.10	25.7	0.55	1.06	1.03	14.8	0.53	1.06	1.03	17.0	**0.61**	1.19	0.97	20.2	0.57	**1.47**	**1.27**	**30.9**
(b)	0.47	0.91	0.84	18.7	0.60	1.39	0.94	22.8	0.58	1.07	0.81	18.9	0.57	1.24	1.06	21.0	0.59	**1.50**	1.23	18.3	**0.61**	1.39	**1.13**	**23.2**
(c)	0.47	1.36	0.98	20.1	0.55	1.67	1.05	20.4	0.56	1.48	1.08	20.5	0.55	1.45	1.09	16.1	0.54	1.11	1.10	18.0	**0.61**	**1.55**	**1.30**	**20.8**
Average	0.47	1.07	0.93	17.5	0.54	1.50	1.03	23.0	0.56	1.20	0.97	18.1	0.55	1.25	1.06	18.0	0.58	1.27	1.10	18.8	**0.60**	**1.47**	**1.23**	**25.0**
Assessments for underwater images with turbrid scene (Fig. 9)																								
	UDCP				RCP				Wavelet-based				IBLA				Fusion-based				Proposed method			
	UCIQE	UIQM	PCQI	MEON	UCIQE	UIQM	PCQI	MEON	UCIQE	UIQM	PCQI	MEON	UCIQE	UIQM	PCQI	MEON	UCIQE	UIQM	PCQI	MEON	UCIQE	UIQM	PCQI	MEON
(a)	0.60	1.14	0.85	22.7	0.57	0.79	1.02	18.0	0.63	1.30	0.91	27.5	0.61	0.92	1.09	23.7	0.60	1.03	0.97	27.9	**0.65**	**1.39**	**1.24**	**40.9**
(b)	0.60	1.10	0.80	32.5	0.59	0.80	1.02	25.7	**0.65**	1.23	0.87	32.8	0.54	0.76	1.01	26.7	0.58	0.93	1.02	28.9	0.62	**1.27**	**1.15**	**33.4**
(c)	0.50	1.08	0.72	11.9	0.53	0.78	0.83	11.3	0.59	0.89	0.90	**11.9**	0.53	0.65	0.94	5.91	**0.61**	0.92	0.98	10.8	0.59	**1.41**	**0.99**	11.2
Average	0.56	1.11	0.79	22.4	0.56	0.79	0.95	18.3	0.62	1.14	0.90	24.1	0.56	0.77	1.01	18.8	0.60	0.96	0.99	22.6	**0.62**	**1.36**	**1.12**	**28.5**
Assessments for underwater images with low-light scene (Fig. 10)																								
	UDCP				RCP				Wavelet-based				IBLA				Fusion-based				Proposed method			
	UCIQE	UIQM	PCQI	MEON	UCIQE	UIQM	PCQI	MEON	UCIQE	UIQM	PCQI	MEON	UCIQE	UIQM	PCQI	MEON	UCIQE	UIQM	PCQI	MEON	UCIQE	UIQM	PCQI	MEON
(a)	0.48	1.50	1.11	17.2	0.54	1.36	1.09	15.1	0.61	1.55	1.29	17.6	0.59	1.55	**1.23**	16.1	0.60	1.42	1.12	17.3	**0.69**	**1.55**	1.15	**17.6**
(b)	0.46	1.40	0.97	26.0	0.54	1.56	1.19	18.6	0.59	1.49	1.17	23.7	0.61	1.54	1.13	21.1	0.67	1.57	1.19	23.7	**0.75**	**1.64**	**1.20**	**33.3**
(c)	0.61	1.64	0.90	31.2	0.61	1.48	0.82	31.2	0.59	**1.75**	0.84	27.8	0.59	1.58	0.75	28.9	0.60	1.53	0.95	36.7	**0.64**	1.63	**1.15**	**41.1**
Average	0.52	1.52	0.99	24.8	0.56	1.47	1.03	21.6	0.60	1.60	1.10	23.0	0.60	1.56	1.04	22.0	0.62	1.51	1.08	25.9	**0.69**	**1.61**	**1.17**	**30.7**
Assessments for underwater images with artificial lighting scene (Fig. 11)																								
	UDCP				RCP				Wavelet-based				IBLA				Fusion-based				Proposed method			
	UCIQE	UIQM	PCQI	MEON	UCIQE	UIQM	PCQI	MEON	UCIQE	UIQM	PCQI	MEON	UCIQE	UIQM	PCQI	MEON	UCIQE	UIQM	PCQI	MEON	UCIQE	UIQM	PCQI	MEON
(a)	0.58	**1.72**	1.04	13.7	0.54	1.56	1.02	11.3	0.57	1.72	0.86	14.7	0.56	1.54	1.14	13.1	0.59	1.65	1.15	11.9	**0.65**	1.70	**1.38**	**17.9**
(b)	0.52	1.26	0.92	20.8	0.54	1.17	0.97	20.7	0.56	1.45	0.90	22.7	0.61	1.18	0.99	25.3	0.57	1.12	1.06	24.7	**0.61**	**1.69**	**1.24**	**33.8**
(c)	0.47	1.01	0.97	20.6	0.58	1.10	1.05	22.4	0.57	1.23	1.00	20.5	0.54	1.10	1.07	20.5	0.60	1.21	1.08	23.0	**0.64**	**1.47**	**1.26**	**27.9**
Average	0.52	1.33	0.98	18.4	0.55	1.28	1.01	18.1	0.56	1.47	0.92	19.3	0.57	1.28	1.07	19.7	0.59	1.32	1.10	19.9	**0.63**	**1.62**	**1.29**	**26.6**

TABLE 3. Quantitative assessments of the 100 raw images extracted from the underwater benchmark dataset [52] using UCIQE [56], UIQM [57], PCQI [58], MEON [59] Metrics. (The bold values express the best metric values).

	UDCP	RCP	Wavelet-based	IBLA	Fusion-based	Proposed method
UCIQE	0.55	0.55	0.60	0.58	0.59	**0.63**
UIQM	1.28	1.29	1.46	1.42	1.39	**1.53**
PCQI	0.94	1.02	1.02	1.05	1.08	**1.23**
MEON	19.47	16.20	20.96	19.69	19.08	**22.91**

TABLE 4. Quantitative statistics of edge pixels and matching feature points obtained from different compared methods. (The bold values express the best metric values).

	Raw image	Untreated	UDCP	RCP	Wavelet-based	IBLA	Fusion-based	Proposed Method
Canny	Fig.13(a)	6956	29962	16238	36316	29802	34560	**55303**
	Fig.13(c)	221	357	3428	2340	1683	10202	**23558**
SURF	Fig.14(a)	193	903	468	1149	920	1382	**1571**
	Fig.14(c)	15	15	129	101	67	432	**544**

Summarizing from the Table 2, the outstanding of PCQI and MEON scores validates the contribution of proposed method to enhance the contrast. Moreover, the scores of UCIQE and UIQM metrics are basically above 0.6 and 1.3, respectively, which further demonstrate the superiority in robustness of the proposed method in dehazing and color correction. In addition, we extract 100 raw underwater images with various challenge scenes are extracted from the underwater benchmark dataset [52] for quantitative comparison. The average values of UCIQE, UIQM, PCIQ and MEON metrics for the 100 restored images produced by all the compared methods are presented in Table 3. Observing form Table 3, we can conclude that our proposed approach outperforms the other state-of-the-art methods in terms of the higher values of these four metrics.

D. APPLICATION TEST

In this section, we employ two widely used image features, known as Canny edge detection [60] and speeded up robust features (SURF) [61] to evaluate the contribution of

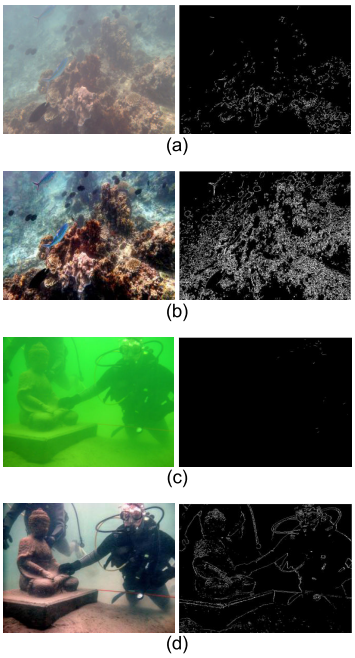

FIGURE 13. Application test using Canny. (a)/(c) Raw images. (b)/(d) the experimental results of enhanced images by proposed method.

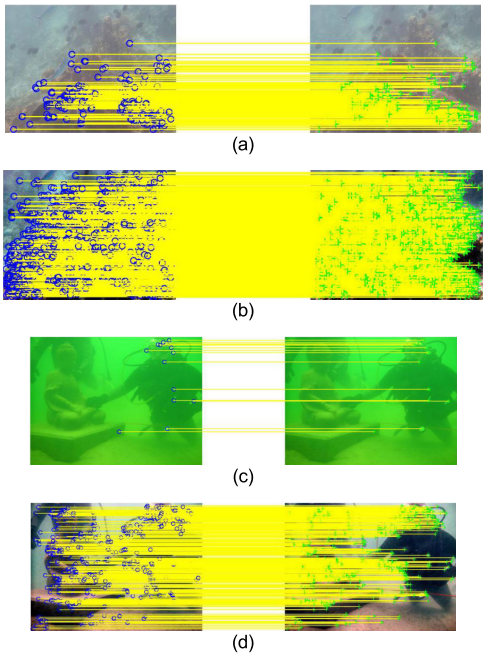

FIGURE 14. Application test using SURF. (a)/(c) Raw images. (b)/(d) the experimental results of enhanced images by proposed method.

our work to computer vision applications. The Canny and SURF operations are both implemented on the original and enhanced images to demonstrate the performance on unveiling structural details. The corresponding experimental results are shown in Fig. 13 and Fig. 14, respectively. To clearly prove the performance of proposed method, the number of detecting edge pixels and matching feature points after using different compared methods are further statistically given in Table 4. It can be easily observed that the amounts of these image features are significantly improved with 10 times after applying the proposed UWB algorithm and VCSE algorithm, which are appreciably higher than other five compared methods. Hence, the effectiveness of the proposed framework is further validated.

V. CONCLUSION AND FUTURE WORK

For underwater image enhancement, we propose a hybrid framework integrating a developed UWB technique and a VCSE model to improve the visual quality of underwater images. These two schemes are initially designed to cope with different degradation problems respectively. Compared with the other five state-of the-art methods, fifteen representative underwater degraded images with different challenge scenes are selected to conduct experiments. The considerably qualitative and quantitative results demonstrate that the proposed method has a better performance on color rendition and visibility improvement. Although the proposed strategy may slightly enhance the noise caused by suspended solids, the excellent natural appearance and detail clarity are sufficient to make up for it. Besides, the proposed hybrid framework can not only provide a good technology to solve the problem of underwater image enhancement, but also expand its applications in underwater computer vision, such as image recognition and target detection.

We are currently working on extension of our framework, including consideration of other factors that may cause the degradation in underwater image. For example, motion blurring, which is a common phenomenon in underwater image, but is rarely mentioned in restoration and enhancement methods. Besides, making our method capable of video processing will be another direction of our future work.

REFERENCES

[1] M. Yang, J. Hu, C. Li, G. Rohde, Y. Du, and K. Hu, "An in-depth survey of underwater image enhancement and restoration," *IEEE Access*, vol. 7, pp. 123638–123657, 2019.
[2] C. Sánchez-Ferreira, L. S. Coelho, H. V. H. Ayala, M. C. Q. Farias, and C. H. Llanos, "Bio-inspired optimization algorithms for real underwater image restoration," *Signal Process., Image Commun.*, vol. 77, pp. 49–65, Sep. 2019.
[3] G. Hou, X. Zhao, Z. Pan, H. Yang, L. Tan, and J. Li, "Benchmarking underwater image enhancement and restoration, and beyond," *IEEE Access*, vol. 8, pp. 122078–122091, 2020.
[4] Q. Jiang, Y. Chen, G. Wang, and T. Ji, "A novel deep neural network for noise removal from underwater image," *Signal Process., Image Commun.*, vol. 87, Sep. 2020, Art. no. 115921.
[5] C. Li, S. Anwar, and F. Porikli, "Underwater scene prior inspired deep underwater image and video enhancement," *Pattern Recognit.*, vol. 98, Feb. 2020, Art. no. 107038.
[6] C. Dai, M. Lin, X. Wu, Z. Wang, and Z. Guan, "Single underwater image restoration by decomposing curves of attenuating color," *Opt. Laser Technol.*, vol. 123, Mar. 2020, Art. no. 105947.
[7] G. Hou, Z. Pan, G. Wang, H. Yang, and J. Duan, "An efficient nonlocal variational method with application to underwater image restoration," *Neurocomputing*, vol. 369, pp. 106–121, Dec. 2019.
[8] B. L. McGlamery, "A computer model for underwater camera systems," *Proc SPIE*, vol. 208, pp. 221–231, Oct. 1979.
[9] J. S. Jaffe, "Computer modeling and the design of optimal underwater imaging systems," *IEEE J. Ocean. Eng.*, vol. 15, no. 2, pp. 101–111, Apr. 1990.
[10] H. Koschmieder, "Theorie der horizontalen sichtweite," *Beitr. Phys. Freien Atmos.*, vol. 12, no. 2, pp. 171–181, 1924.

[11] C. Chen, S. Li, Y. Wang, H. Qin, and A. Hao, "Video saliency detection via spatial-temporal fusion and low-rank coherency diffusion," *IEEE Trans. Image Process.*, vol. 26, no. 7, pp. 3156–3170, Jul. 2017.

[12] P. Gao, H. Zhang, J. Yu, J. Lin, X. Wang, M. Yang, and F. Kong, "Secure cloud-aided object recognition on hyperspectral remote sensing images," *IEEE Internet Things J.*, to be published.

[13] Y. Li, S. Li, C. Chen, A. Hao, and H. Qin, "A plug-and-play scheme to adapt image saliency deep model for video data," *IEEE Trans. Circuits Syst. Video Technol.*, early access, Sep. 10, 2020, doi: 10.1109/TCSVT.2020.3023080.

[14] B. Huang, Z. Pan, H. Yang, and L. Bai, "Variational level set method for image segmentation with simplex constraint of landmarks," *Signal Process., Image Commun.*, vol. 82, Mar. 2020, Art. no. 115745.

[15] K. Li, S. Qi, H. Yang, L. Zhou, and D. Song, "Extensible image object co-segmentation with sparse cooperative relations," *Inf. Sci.*, vol. 521, pp. 422–434, Jun. 2020.

[16] W. Hou, D. J. Gray, A. D. Weidemann, G. R. Fournier, and J. L. Forand, "Automated underwater image restoration and retrieval of related optical properties," in *Proc. IEEE Int. Geosci. Remote Sens. Symp.*, Jul. 2007, pp. 1889–1892.

[17] N. Carlevaris-Bianco, A. Mohan, and R. M. Eustice, "Initial results in underwater single image dehazing," in *Proc. OCEANS MTS/IEEE SEATTLE*, Seattle, WA, USA, Sep. 2010, pp. 1–8.

[18] H. Lu, Y. Li, L. Zhang, and S. Serikawa, "Contrast enhancement for images in turbid water," *J. Opt. Soc. Amer. A, Opt. Image Sci.*, vol. 32, no. 5, pp. 886–893, 2015.

[19] Y.-T. Peng and P. C. Cosman, "Underwater image restoration based on image blurriness and light absorption," *IEEE Trans. Image Process.*, vol. 26, no. 4, pp. 1579–1594, Apr. 2017.

[20] D. Berman, T. Treibitz, and S. Avidan, "Diving into haze-lines: Color restoration of underwater images," *Proc. Briti. Mach. Vis. Conf. (BMVC)*, London, U.K., 2017, pp. 1–12.

[21] Y. Wang, H. Liu, and L.-P. Chau, "Single underwater image restoration using adaptive attenuation-curve prior," *IEEE Trans. Circuits Syst. I, Reg. Papers*, vol. 65, no. 3, pp. 992–1002, Mar. 2018.

[22] Y. Y. Schechner, S. G. Narasimhan, and S. K. Nayar, "Instant dehazing of images using polarization," in *Proc. IEEE Comput. Soc. Conf. Comput. Vis. Pattern Recognit. (CVPR)*, Kauai, HI, USA, Dec. 2001, p. 325.

[23] L. Shen, Y. Zhao, Q. Peng, J. C.-W. Chan, and S. G. Kong, "An iterative image dehazing method with polarization," *IEEE Trans. Multimedia*, vol. 21, no. 5, pp. 1093–1107, May 2019.

[24] K. He, J. Sun, and X. Tang, "Single image haze removal using dark channel prior," *IEEE Trans. Pattern Anal. Mach. Intell.*, vol. 33, no. 12, pp. 2341–2353, Dec. 2011.

[25] R. W. Liu, S. Xiong, and H. Wu, "A second-order variational framework for joint depth map estimation and image dehazing," in *Proc. IEEE Int. Conf. Acoust., Speech Signal Process. (ICASSP)*, Calgary, AB, Canada, Apr. 2018, pp. 1433–1437.

[26] Q. Shu, C. Wu, Q. Zhong, and R. W. Liu, "Alternating minimization algorithm for hybrid regularized variational image dehazing," *Optik*, vol. 185, pp. 943–956, May 2019.

[27] Z. Wang, G. Hou, Z. Pan, and G. Wang, "Single image dehazing and denoising combining dark channel prior and variational models," *IET Comput. Vis.*, vol. 12, no. 4, pp. 393–402, Jun. 2018.

[28] J. Y. Chiang and Y.-C. Chen, "Underwater image enhancement by wavelength compensation and dehazing," *IEEE Trans. Image Process.*, vol. 21, no. 4, pp. 1756–1769, Apr. 2012.

[29] P. L. J. Drews, E. R. Nascimento, S. S. C. Botelho, and M. F. M. Campos, "Underwater depth estimation and image restoration based on single images," *IEEE Comput. Graph. Appl.*, vol. 36, no. 2, pp. 24–35, Mar. 2016.

[30] A. Galdran, D. Pardo, A. Picón, and A. Alvarez-Gila, "Automatic red-channel underwater image restoration," *J. Vis. Commun. Image Represent.*, vol. 26, pp. 132–145, Jan. 2015.

[31] Y.-T. Peng, K. Cao, and P. C. Cosman, "Generalization of the dark channel prior for single image restoration," *IEEE Trans. Image Process.*, vol. 27, no. 6, pp. 2856–2868, Jun. 2018.

[32] G. Hou, J. Li, G. Wang, Z. Pan, and X. Zhao, "Underwater image dehazing and denoising via curvature variation regularization," *Multimedia Tools Appl.*, vol. 79, nos. 27–28, pp. 20199–20219, Apr. 2020.

[33] R. Hummel, "Image enhancement by histogram transformation," *Comput. Graph. Image Process.*, vol. 6, no. 2, pp. 184–195, Apr. 1977.

[34] X. Fu and X. Cao, "Underwater image enhancement with global–local networks and compressed-histogram equalization," *Signal Process., Image Commun.*, vol. 86, Aug. 2020, Art. no. 115892.

[35] G. Buchsbaum, "A spatial processor model for object colour perception," *J. Franklin Inst.*, vol. 310, no. 1, pp. 1–26, Jul. 1980.

[36] M. Ebner, *Color Constancy*, 1st ed. Hoboken, NJ, USA: Wiley, 2007.

[37] J. van de Weijer, T. Gevers, and A. Gijsenij, "Edge-based color constancy," *IEEE Trans. Image Process.*, vol. 16, no. 9, pp. 2207–2214, Sep. 2007.

[38] G. N. Lan, J. Li, and F. Ji, "Underwater image backscatter noise reduction based on wavelets," *Ocean Technol.*, vol. 29, no. 2, pp. 43–47, Feb. 2010.

[39] G. Hou, Z. Pan, B. Huang, G. Wang, and X. Luan, "Hue preserving-based approach for underwater colour image enhancement," *IET Image Process.*, vol. 12, no. 2, pp. 292–298, Feb. 2018.

[40] Y. Guo, Y. Lu, R. W. Liu, M. Yang, and K. T. Chui, "Low-light image enhancement with regularized illumination optimization and deep noise suppression," *IEEE Access*, vol. 8, pp. 145297–145315, 2020.

[41] K. Iqbal, R. A. Salam, A. Osman, and A. Z. Talib, "Underwater image enhancement using an integrated colour model," *IAENG Int. J. Comput. Sci.*, vol. 34, no. 2, pp. 239–244, 2007.

[42] C. O. Ancuti, C. Ancuti, T. Haber, and P. Bekaert, "Fusion-based restoration of the underwater images," in *Proc. 18th IEEE Int. Conf. Image Process.*, Sep. 2011, pp. 1557–1560.

[43] X. Fu, P. Zhuang, Y. Huang, Y. Liao, X.-P. Zhang, and X. Ding, "A retinex-based enhancing approach for single underwater image," in *Proc. IEEE Int. Conf. Image Process. (ICIP)*, Paris, France, Oct. 2014, pp. 4572–4576.

[44] T. Ji and G. Wang, "An approach to underwater image enhancement based on image structural decomposition," *J. Ocean Univ. China*, vol. 14, no. 2, pp. 255–260, Apr. 2015.

[45] A. S. A. Ghani and N. A. M. Isa, "Underwater image quality enhancement through composition of dual-intensity images and Rayleigh-stretching," in *Proc. IEEE 4th Int. Conf. Consum. Electron. Berlin (ICCE-Berlin)*, Berlin, Germany, Sep. 2014, pp. 219–230.

[46] A. S. Abdul Ghani and N. A. Mat Isa, "Underwater image quality enhancement through integrated color model with Rayleigh distribution," *Appl. Soft Comput.*, vol. 27, pp. 219–230, Feb. 2015.

[47] X. Fu, Z. Fan, M. Ling, Y. Huang, and X. Ding, "Two-step approach for single underwater image enhancement," in *Proc. Int. Symp. Intell. Signal Process. Commun. Syst. (ISPACS)*, Xiamen, China, Nov. 2017, pp. 789–794.

[48] C. Li, J. Guo, and C. Guo, "Emerging from water: Underwater image color correction based on weakly supervised color transfer," *IEEE Signal Process. Lett.*, vol. 25, no. 3, pp. 323–327, Mar. 2018.

[49] C.-Y. Li, J.-C. Guo, R.-M. Cong, Y.-W. Pang, and B. Wang, "Underwater image enhancement by dehazing with minimum information loss and histogram distribution prior," *IEEE Trans. Image Process.*, vol. 25, no. 12, pp. 5664–5677, Dec. 2016.

[50] C. O. Ancuti, C. Ancuti, C. De Vleeschouwer, and P. Bekaert, "Color balance and fusion for underwater image enhancement," *IEEE Trans. Image Process.*, vol. 27, no. 1, pp. 379–393, Jan. 2018.

[51] X. X. Zhao, C. Y. Heng, L. C. J. K. Jiang Bin, and S. L. Sun, "Color cast detection and color correction methods based on image analysis," *Meas. Control Technol*, vol. 27, no. 5, pp. 10–14, May 2008.

[52] C. Y. Li, C. L. Guo, W. Q. Ren, R. M. Cong, J. H. Hou, S. Kwong, and D. C. Tao, "An underwater image enhancement benchmark dataset and beyond," *IEEE Trans. Image Process.*, vol. 29, no. 12, pp. 2387–2390, Oct. 2015.

[53] M. Bertalmio, V. Caselles, E. Provenzi, and A. Rizzi, "Perceptual color correction through variational techniques," *IEEE Trans. Image Process.*, vol. 16, no. 4, pp. 1058–1072, Apr. 2007.

[54] L. Kwon Choi, J. You, and A. C. Bovik, "Referenceless prediction of perceptual fog density and perceptual image defogging," *IEEE Trans. Image Process.*, vol. 24, no. 11, pp. 3888–3901, Nov. 2015.

[55] X. Liu, H. Zhang, Y.-M. Cheung, X. You, and Y. Y. Tang, "Efficient single image dehazing and denoising: An efficient multi-scale correlated wavelet approach," *Comput. Vis. Image Understand.*, vol. 162, pp. 23–33, Sep. 2017.

[56] M. Yang and A. Sowmya, "An underwater color image quality evaluation metric," *IEEE Trans. Image Process.*, vol. 24, no. 12, pp. 6062–6071, Dec. 2015.

[57] K. Panetta, C. Gao, and S. Agaian, "Human-visual-system-inspired underwater image quality measures," *IEEE J. Ocean. Eng.*, vol. 41, no. 3, pp. 541–551, Jul. 2016.

[58] S. Wang, K. Ma, H. Yeganeh, Z. Wang, and W. Lin, "A patch-structure representation method for quality assessment of contrast changed images," *IEEE Signal Process. Lett.*, vol. 22, no. 12, pp. 2387–2390, Dec. 2015.

[59] K. Ma, W. Liu, K. Zhang, Z. Duanmu, Z. Wang, and W. Zuo, "End-to-end blind image quality assessment using deep neural networks," *IEEE Trans. Image Process.*, vol. 27, no. 3, pp. 1202–1213, Mar. 2018.
[60] J. Canny, "A computational approach to edge detection," *IEEE Trans. Pattern Anal. Mach. Intell.*, vol. PAMI-8, no. 6, pp. 679–698, Nov. 1986.
[61] H. Bay, A. Ess, T. Tuytelaars, and L. V. Gool, "Speed up robust feature (SURF)," *Comput Vis. Image Underst.*, vol. 110, no. 3, pp. 346–359, Jun. 2008.

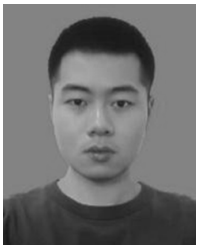

XINJIE LI received the B.S. degree in software engineering from Qingdao University, in 2018, where he is currently pursuing the master's degree. His research interests include image processing and computer vision.

GUOJIA HOU (Member, IEEE) received the B.S. degree in computer science, and the M.S. and Ph.D. degrees in computer applications technology from the Ocean University of China, in 2010, 2012, and 2015, respectively. He is currently an Associate Professor with the College of Computer Science and Technology, Qingdao University. His research interests include image processing and pattern recognition.

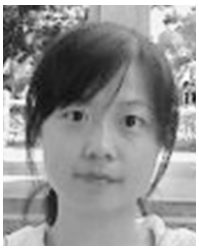

LU TAN received the B.Sc. degree in electronic information engineering from the Qingdao University of Science and Technology, China, in 2010, and the M.Sc. degree in computer science and technology from Qingdao University, China, in 2016. She is currently pursuing the Ph.D. degree with the School of Electrical Engineering, Computing and Mathematical Sciences (Computing Discipline), Curtin University, Australia. Her current research interests include variational image restoration and segmentation, illusory contour capture, intelligent video analysis, and 3-D medical image processing.

WANQUAN LIU (Senior Member, IEEE) received the B.Sc. degree in applied mathematics from Qufu Normal University, China, in 1985, the M.Sc. degree in control theory and operation research from the Chinese Academy of Science, in 1988, and the Ph.D. degree in electrical engineering from Shanghai Jiao Tong University, in 1993. He has held the ARC Fellowship, U2000 Fellowship, and JSPS Fellowship and attracted research funds from different resources over 2.4 million dollars. He is currently an Associate Professor with the Department of Computing, Curtin University. He is in editorial board of nine international journals. His current research interests include large-scale pattern recognition, signal processing, machine learning, and control systems.